A Passive Lossless Snubber Cell for Nonisolated PWM DC/DC Converters

Ching-Jung Tseng and Chern-Lin Chen, *Member, IEEE*

***Abstract*—A passive lossless snubber cell is proposed to improve the turn-on and turnoff transients of the MOSFET's in nonisolated pulsewidth modulated (PWM) dc/dc converters. Switching losses and EMI noise are reduced by restricting di/dt of the reverse-recovery current and dv/dt of the drain–source voltage. The MOSFET operates at zero-voltage-switching (ZVS) turnoff and near zero-current-switching (ZCS) turn-on. The freewheeling diode is also commutated under ZVS. As an example, operation principles, theoretical analysis, relevant equations, and experimental results of a boost converter equipped with the proposed snubber cell are presented in detail. Efficiency of 96% has also been measured in the experimental results reported for a 1-kW 100-kHz prototype in the laboratory. Six basic nonisolated PWM dc/dc converters (buck, boost, buck-boost, Cúk, Sepic, and Zeta) equipped with the proposed general snubber cells are also shown in this paper.**

***Index Terms*— Converters, pulsewidth modulation, switching circuits.**

I. Introduction

PULSEWIDTH modulated (PWM) dc/dc converters have been widely used as switched-mode power supplies in industry. The PWM technique is praised for its high power capability and ease of control. Higher power density and faster transient response of PWM dc/dc converters can be achieved by increasing the switching frequency. However, as the switching frequency increases, so do the switching losses and EMI noise. High switching losses reduce the power capabilities, while serious EMI noise interferes with the control of PWM dc/dc converters.

Switching losses and EMI noise of PWM dc/dc converters are mainly generated during turn-on and turnoff switching transients. According to [1], there are three nonideal commutation phenomena when MOSFET's are used as power switches.

1) A surge current flows through the MOSFET, caused by the reverse-recovery current of the freewheeling diode during the turn-on process. This is the dominant source of turn-on loss and di/dt EMI noise.
2) Discharge of the parasitic drain–source capacitance of the MOSFET occurs during the turn-on process. This mechanism can be eliminated only by resonant converter techniques or active snubbers.

Manuscript received May 22, 1997; revised March 19, 1998. Abstract published on the Internet May 1, 1998.

The authors are with the Power Electronics Laboratory, Department of Electrical Engineering, National Taiwan University, Taipei, 10764 Taiwan, R.O.C.

Publisher Item Identifier S 0278-0046(98)05680-9.

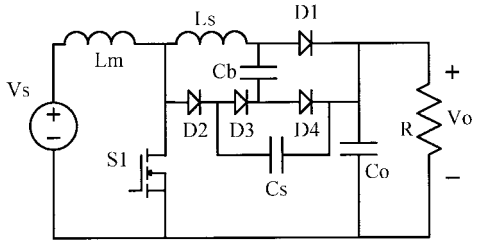

Fig. 1. A boost converter with the passive lossless snubber.

3) Fast increase of the drain–source voltage during the turnoff process occurs. This is the source of dv/dt EMI noise and turnoff loss.

To improve the problems resulting from the nonideal phenomena described above, several kinds of soft-switching technologies have been presented in the literature [2]–[13]. Active snubbers, as introduced in [2]–[5], can reduce all three loss mechanisms by using auxiliary switches. Unfortunately, an auxiliary switch increases the complexity of both power and control circuits. Synchronization problems between control signals of the two switches during transient also complicate the control strategy. The circuit cost is increased and the reliability is decreased by using active snubbers. Resistors, capacitors, and diodes (RCD) snubbers in [6] have the simplest structures and, hence, the lowest costs. However, they also have the worst performance, since the switching losses are dissipated in resistors and, thus, reduce the efficiency of the circuit. Resonant converters in [7] and [8] commutate with either zero voltage switching (ZVS) or zero current switching (ZCS) to reduce switching losses. However, conduction losses are increased due to the high circulating current involved. It is also hard to design an EMI filter and control circuit because of a wide switching frequency range. Compared with the three technologies discussed above, a passive lossless snubber can effectively restrict switching losses and EMI noise using no active components and no power dissipative components [9]–[13]. Increasing the rates of the drain current and the drain–source voltage are restricted by inductors and capacitors, respectively. The control strategy is scarcely interfered with and the circulating energy generated is comparatively low. The circuit structure is as simple as RCD snubbers and the efficiency is as high as active snubbers and resonant converters. Low cost, high performance, and high reliability are the distinct advantages of a passive lossless snubber.

As an example, a boost converter equipped with the proposed snubber cell is investigated in depth. Snubber operation principles are analyzed and component parameters can be

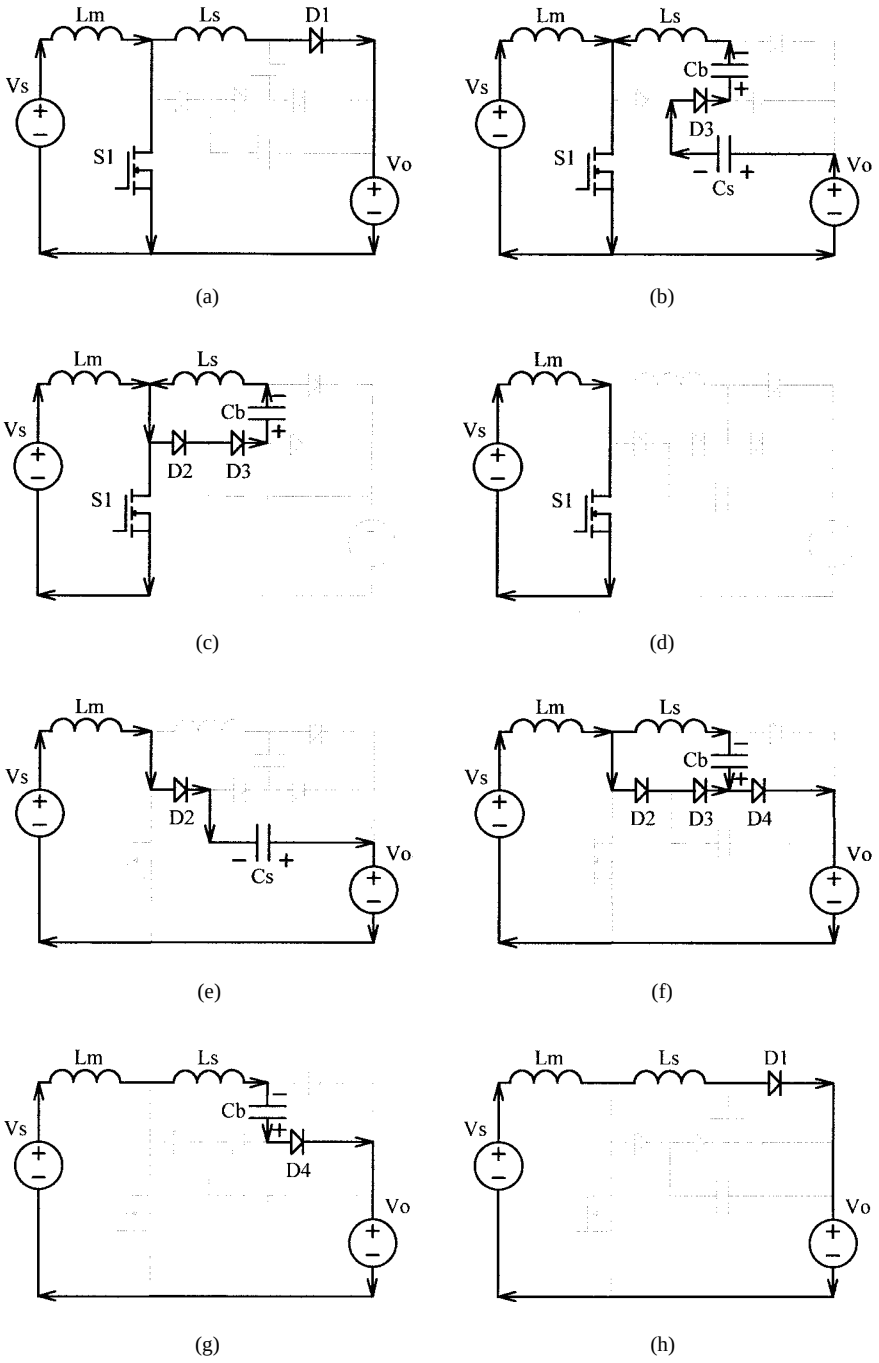

Fig. 2. Equivalent circuits during one switching cycle. (a) Stage 1 (S_1 on). (b) Stage 2 (D_1 off, D_3 on). (c) Stage 3 (D_2 on). (d) Stage 4 (D_2, D_3 off). (e) Stage 5 (S_1 off, D_2 on). (f) Stage 6 (D_3, D_4 on). (g) Stage 7 (D_2, D_3 off). (h) Stage 8 (D_1 on, D_4 off).

mathematically determined. Experimental results of a 1-kW 100-kHz boost converter are used to verify the analysis. Formation of the general snubber cell is also discussed. Six basic nonisolated PWM dc/dc converters equipped with the proposed snubber cells are illustrated in this paper.

II. A Boost Converter with the Proposed Snubber Cell

A. Principle of Operation

Shown in Fig. 1 is a boost converter with the proposed passive lossless snubber cell, which is encircled by dotted lines. During the turn-on process, injected charges in the low-doped middle region of diode D_1 cause transient reverse-recovery current flowing reversely through diode D_1. The surge current is the major part of the switching losses. Increasing the rate of the reverse-recovery current is restricted by the snubber inductor L_s to suppress the switching loss. The MOSFET commutates near ZCS turn-on, since part of the turn-on loss resulting from the discharge of the parasitic drain–source capacitance cannot be removed by a passive snubber.

During the turnoff process, the drain–source voltage increases immediately to the output voltage. Fast dv/dt increases

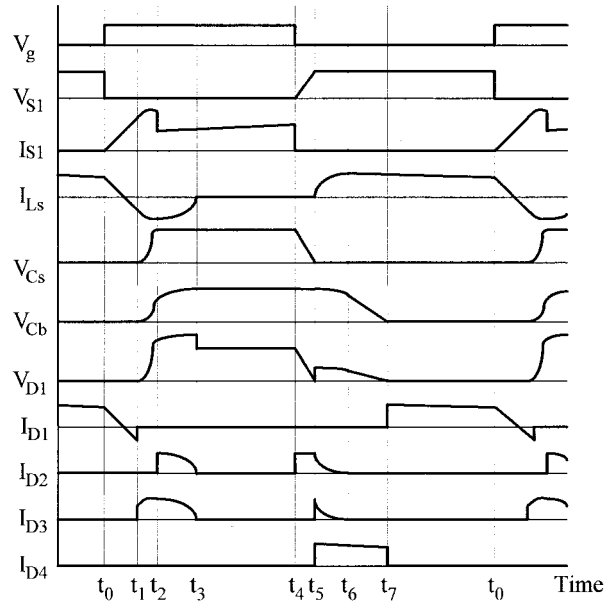

Fig. 3. Key waveforms of the boost converter with the passive lossless snubber cell.

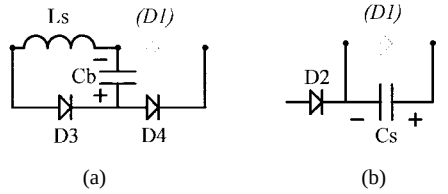

Fig. 4. General passive lossless turn-on and turnoff snubber cell. (a) Turn-on snubber cell. (b) Turnoff snubber cell.

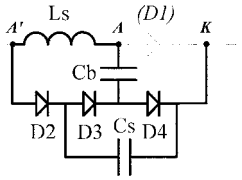

Fig. 5. The general passive lossless snubber cell proposed for nonisolated PWM dc/dc converters.

the turnoff loss and, of more importance, it generates serious EMI noise. Increasing the rate of the drain–source voltage is restricted by the snubber capacitor C_s to obtain ZVS turnoff and to reduce EMI noise. Notice that the freewheeling diode is also commutated under ZVS during both turn-on and turnoff.

Turn-on and turnoff switching losses are reduced by the snubber inductor and the snubber capacitor, respectively. The energy transferred to the buffer capacitor C_b can be viewed as the summation of the energy absorbed in snubber inductor L_s and snubber capacitor C_s. Energy recovery is achieved by discharging the buffer capacitor C_b to the output. Ideally, no power is dissipated or accumulated in the passive components of this snubber.

TABLE I
PARTS LIST OF THE IMPLEMENTED PROTOTYPE POWER CIRCUIT

Part	Type	Part	Value
S	IRFP460	L_s	5uH
D_1	HFA15TB60	C_s	3.3nF
D_2	HFA15TB60	C_b	100nF
D_3	HFA15TB60	L	180uH
D_4	HFA15TB60	C	940uF

B. Equivalent Circuit Analysis

To analyze the steady-state operation of the circuit shown in Fig. 1, the following assumptions are made during one switching cycle.

1) The output capacitor C_o is large enough to assume that the output voltage V_o is constant and ripple free.
2) Input voltage V_s is constant.
3) All semiconductor devices are ideal, except the freewheeling diode D_1.
4) Main inductor L_m is much greater than snubber inductor L_s.

Based on these assumptions, circuit operation in one switching cycle can be divided into eight stages, as shown in Fig. 2(a)–(h), respectively.

Combining the turn-on and turnoff snubber cells described above, the proposed passive lossless snubber cell for nonisolated PWM dc/dc converters is defined and shown in Fig. 5. Node $\boldsymbol{A}$ and $\boldsymbol{K}$ are connected to the anode and the cathode of the converter freewheeling diode D_1, respectively. Node $\boldsymbol{A'}$ is connected to the component which is connected to the anode of the freewheeling diode.

Stage 1 [Fig. 2(a); $t_0 < t < t_1$]: S_1 turns on at t_0. During the turn-on process, D_1 is not immediately turned off because of the reverse-recovery phenomenon. Increasing the rate of the drain current is restricted by the snubber inductor to achieve ZCS turn-on of the MOSFET. The current of the snubber inductor L_s is given by

$$I_{Ls}(t) = I_{Lm}(t_0) - \frac{V_O}{L_S}(t - t_0). \tag{1}$$

Stage 2 [Fig. 2(b); $t_1 < t < t_2$]: The reverse-recovery phenomenon finishes at t_1. As soon as D_1 is turned off, diode D_3 is naturally turned on, because V_{C_s} and V_{C_b} are equal to zero. Snubber inductor L_s, snubber capacitor C_s, and buffer capacitor C_b are charged by the output through the first resonant path $V_o - C_s - D_3 - C_b - L_s - S_1$. Increasing the rate of the voltage across D_1, which is equal to $V_{C_s} + V_{C_b}$, is restricted to achieve ZVS turnoff of the freewheeling diode D_1. Snubber inductor current, snubber capacitor voltage, and buffer capacitor voltage are

$$I_{Ls}(t) = -\frac{V_O}{Z_1}\sin(\omega_1(t - t_1)) - I_{rr}\cos(\omega_1(t - t_1)) \tag{2}$$

$$V(t) = I_{rr}Z_1\sin(\omega_1(t - t_1) - V_O\cos(\omega_1(t - t_1)) + V_O \tag{3}$$

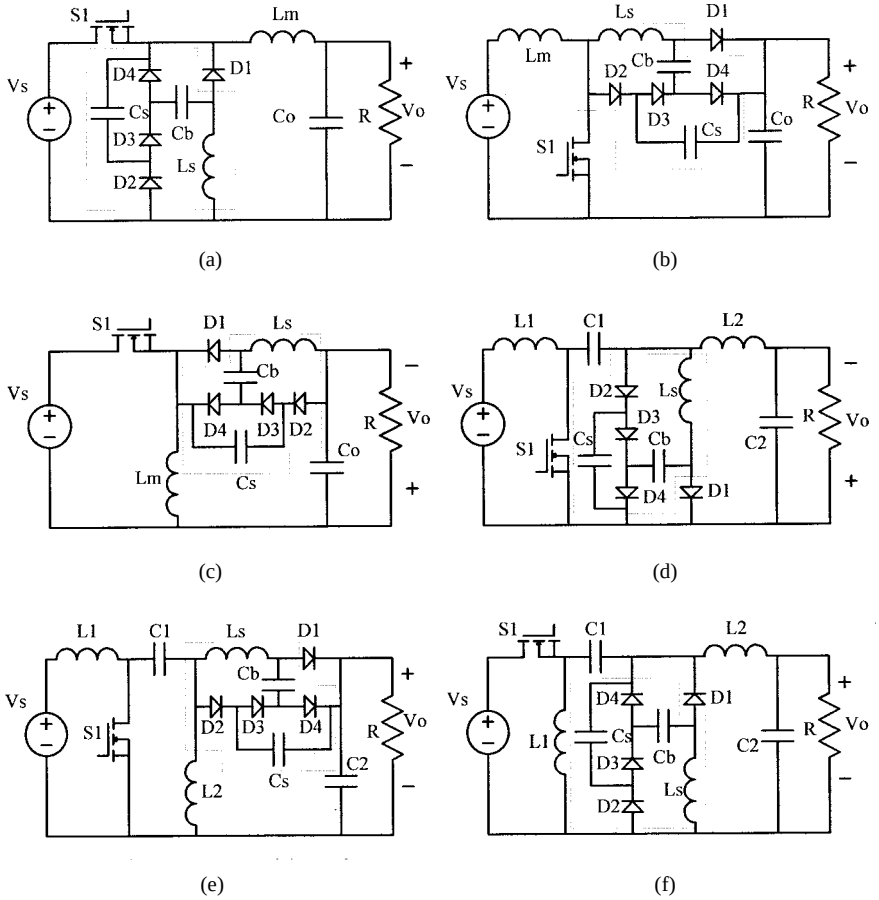

Fig. 6. Six basic nonisolated PWM dc/dc converters with the proposed snubber cells. (a) Buck converter with snubber. (b) Boost converter with snubber. (c) Buck-boost converter with snubber. (d) Cúk converter with snubber. (e) Sepic converter with snubber. (f) Zeta converter with snubber.

$$V_{Cs}(t)=\frac{C_b}{C_S+C_b}V(t),\quad V_{Cb}(t)=\frac{C_S}{C_S+C_b}V(t) \tag{4}$$

where

$$I_{rr}=\frac{V_O}{L_S}(t_1-t_0)-I_{Lm}(t_0) \tag{5}$$

$$Z_1=\sqrt{\frac{L_S(C_S+C_b)}{C_SC_b}} \tag{6}$$

$$\omega_1=\sqrt{\frac{C_S+C_b}{L_SC_S+C_b}}. \tag{7}$$

Peak drain current of the switch S_1 is obtained by the summation of main inductor current I_{Lm} and peak snubber inductor current $I_{Ls,p}$. $I_{Ls,p}$ appears when $V_{Cb}+V_{Cs}$ is equal to V_o, and it is given by

$$I_{Ls,p}=\frac{\sqrt{V_O^2+(I_{rr}Z_1)^2}}{Z_1}. \tag{8}$$

The first resonance stops at t_2 when $V_{Cs}(t_2)$ equals V_o, because diode D_2 is turned on. By using the reciprocity theorem, snubber inductor current at t_2 is given by

$$I_{Ls}(t_2)=\frac{\sqrt{(I_{rr}Z_1)^2+V_O^2-\left(V_O\dfrac{C_S}{C_b}\right)^2}}{Z_1}. \tag{9}$$

From (9), the energy stored in L_s and C_s can be given by

$$\begin{aligned}E_{Ls}(t_2)+E_{Cb}(t_2)&=\tfrac{1}{2}L_SI_{Ls}^2(t_2)+\tfrac{1}{2}C_bV_{Cb}^2(t_2)\\&=\tfrac{1}{2}L_SI_{rr}^2+\tfrac{1}{2}C_SV_O^2.\end{aligned} \tag{10}$$

Stage 3 [Fig. 2(c); $t_2<t<t_3$]: After V_{Cs} is charged to the output voltage level at t_2, D_2 is turned on and V_{Cs} keeps constant. The current in L_s starts to charge C_b through the second resonant path $L_s-D_2-D_3-C_b$. L_s and C_b are performing one-way resonance because of diodes D_2 and D_3. The current through L_s and the voltage across C_b are given by

$$I_{Ls}(t)=\frac{C_S}{C_b}\frac{V_O}{Z_2}\sin(\omega_2(t-t_2))-I_{S2}\cos(\omega_2(t-t_2)) \tag{11}$$

$$V_{Cb}(t)=I_{S2}Z_2\sin(\omega_2(t-t_2))+\frac{C_S}{C_b}V_O\cos(\omega_2(t-t_2)) \tag{12}$$

where

$$I_{S2}=\frac{V_O}{Z_1}\sin(\omega_1(t_2-t_1))+I_{rr}\cos(\omega_1(t_2-t_1)) \tag{13}$$

$$Z_2=\sqrt{\frac{L_S}{C_b}} \tag{14}$$

$$\omega_2=\sqrt{\frac{1}{L_SC_b}}. \tag{15}$$

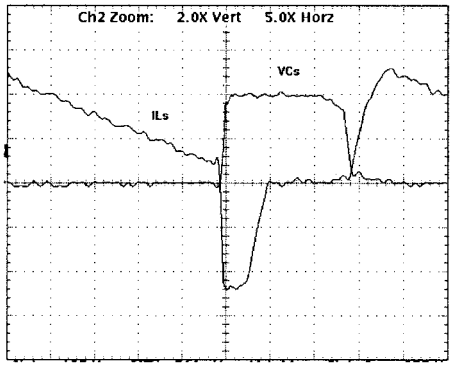

(a)

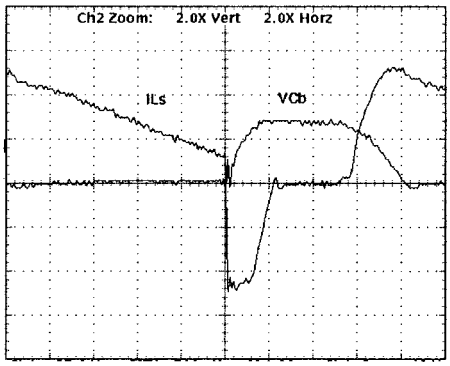

(b)

Fig. 7. Waveforms of snubber inductor current I_{Ls}, snubber capacitor voltage V_{Cs}, and buffer capacitor voltage V_{Cb}. V_{Cs}: 200 V/div; V_{Cb}: 25 V/div; I_{Ls}: 2 A/div; Time 1 μs/div. (a) Waveforms of I_{Ls} and V_{Cs}. (b) Waveforms of I_{Ls} and V_{Cb}.

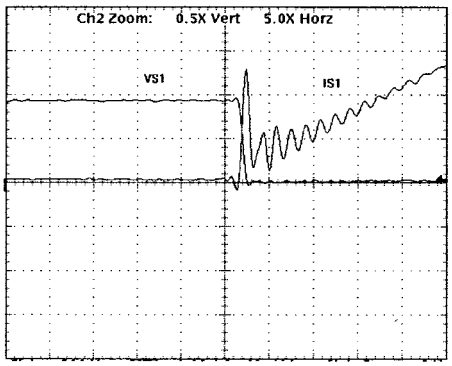

(a)

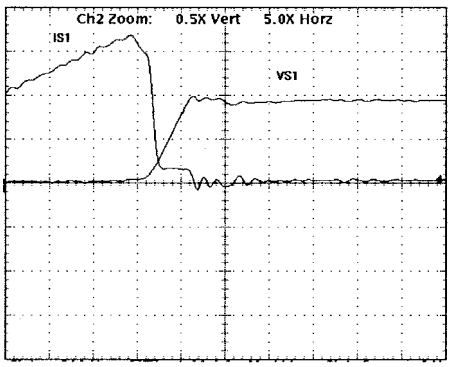

(b)

Fig. 8. Commutation waveforms of MOSFET with snubber. V_{S1}: 200 V/div; I_{S1}: 2 A/div; Time 1 μs/div. (a) Turn-on transients. (b) Turnoff transients.

The second resonance stops at t_3 when $I_{Ls}(t_3)$ becomes 0. Since the energy in L_s is completely transferred to C_b in this stage, the energy stored in C_b at t_3 can be found following (10) to be

$$\begin{aligned}\tfrac{1}{2}\,C_bV_{Cb}^2(t_3) &= E_{Cb(t3)} = E_{Ls(t2)} + E_{Cb(t2)} \\ &= \tfrac{1}{2}\,L_SI_{rr}^2 + \tfrac{1}{2}\,C_SV_O^2. \end{aligned} \tag{16}$$

Also, the peak buffer capacitor voltage $V_{Cb,p}$ is given by

$$V_{Cb,p} = V_{Cb}(t_3) = \sqrt{\frac{L_SI_{rr}^2 + C_SV_O^2}{C_b}}. \tag{17}$$

It also determines the voltage stress of the freewheeling diode, which is equal to V_o plus $V_{Cb,p}$.

Stage 4 [Fig. 2(d); $t_3 < t < t_4$]: At t_3, I_{Ls} is decreased to zero, while D_2 and D_3 are turned off simultaneously. The current through L_s keeps zero and the voltage across C_b keeps constant after t_3. From (16), the total energy transferred to C_b can be viewed as the summation of the energy which was absorbed in L_s and C_s.

Stage 5 [Fig. 2(e); $t_4 < t < t_5$]: After the switch S_1 turns off at t_4, main inductor current $I_{Lm}(t_4)$ flows through D_2 to discharge C_s to the output. D_3 and D_4 are not turned on because they are reverse biased by V_{Cs}. The drain–source voltage of S_1 is equal to $V_o - V_{Cs}$. Slower dv/dt of the drain–source voltage is obtained while V_{Cs} is discharged from V_o to 0. Assuming that I_{Lm} is constant during this stage, V_{Cs} is given by

$$V_{Cs}(t) = V_O - \frac{I_{Lm}(t_4)}{C_S}(t - t_4). \tag{18}$$

Stage 6 [Fig. 2(f); $t_5 < t < t_6$]: Diodes D_3 and D_4 are turned on by the main inductor current $I_{Lm}(t_5)$ when V_{Cs} is discharged to zero at t_5. Voltage across L_s is equal to V_{Cb} and, thus, I_{Ls} increases to discharge C_b to the output. Circuit operation is similar to the second resonance in *Stage 2*. I_{Ls} and V_{Cb} are given by

$$I_{Ls}(t) = \frac{V_{Cb}(t_2)}{Z_2}\sin\left(\omega_2(t - t_5)\right) \tag{19}$$

$$V_{Cb}(t) = V_{Cb}(t_2)\cos\left(\omega_2(t - t_5)\right). \tag{20}$$

Stage 7 [Fig. 2(g); $t_6 < t < t_7$]: I_{Ls} is increased to $I_{Lm}(t_6)$ at $t_6; D_2$, and D_3 are turned off. After t_6, I_{Lm} discharges C_b to the output through D_4. Assuming that I_{Lm} is constant in this stage, V_{Cb} is given by

$$V_{Cb}(t) = V_{Cb}(t_6) - \frac{I_{Lm}(t_6)}{C_b}(t - t_6). \tag{21}$$

ZVS turn-on of diode D_1 is achieved by slow dv/dt of V_{Cb}.

Stage 8 [Fig. 2(h); $t_7 < t < t_0$]: V_{Cb} is discharged to zero at t_7. D_4 is turned off and D_1 is turned on. The energy recovery process of the snubber is finished when all energy in the buffer capacitor C_b is transferred to the output. After that,

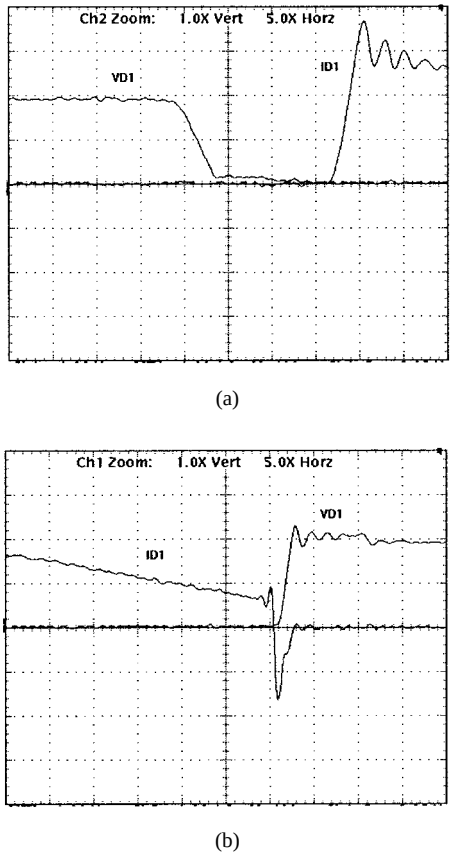

Fig. 9. Commutation waveforms of freewheeling diode with snubber. V_{D1}: 200 V/div; I_{D1}: 2 A/div; Time 1 μs/div. (a) Turn-on transients. (b) Turnoff transients.

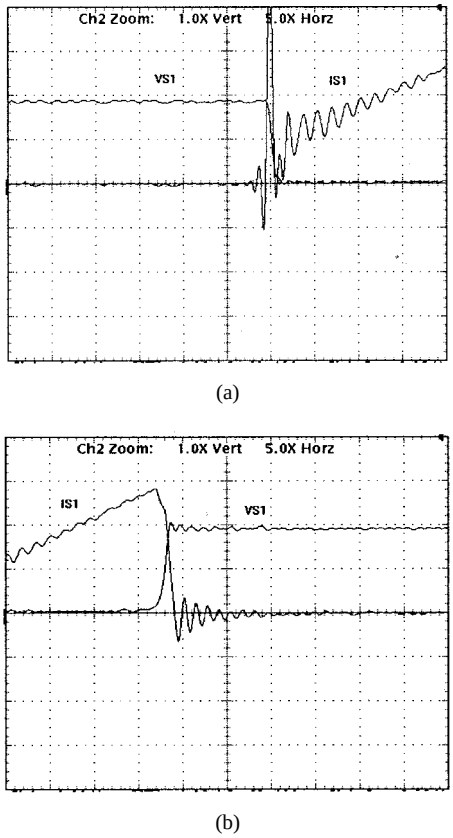

Fig. 10. Commutation waveforms of MOSFET without snubber. V_{S1}: 200 V/div; I_{S1}: 2 A/div; Time 1 μs/div. (a) Turn-on transients. (b) Turnoff transients.

main inductor current I_{Lm} flows through diode D_1 instead of diode D_4 to prevent C_s from being charged reversely. Circuit operation will be the same as in *Stage 1* when the switch S_1 turns on again at t_0 in the next switching cycle.

Based on the analysis presented above, key waveforms of the boost converter with the proposed snubber cell are shown in Fig. 3.

C. Design Considerations

The snubber inductor L_s, snubber capacitor C_s, and buffer capacitor C_b are the three main elements to be designed. The following rules should be noted when designing L, C values.

1) In *Stage 6*, diodes D_2 and D_3 should be naturally turned off before the voltage of C_b is discharged to zero, or the residential current will turn on D_2, D_3, and D_4 in the entire switching period. In other words, the following inequality has to be obeyed:

$$\tfrac{1}{2} L_S I_F^2 < \tfrac{1}{2} L_S I_{rr}^2 + \tfrac{1}{2} C_S V_O^2. \tag{22}$$

It requires higher I_{rr} or larger C_s.

2) Current stress of the MOSFET and voltage stress of the freewheeling diode are given in (8) and (17), respectively. Larger C_s results in higher MOSFET current stress and higher diode voltage stress.
3) According to (17), C_b has to be at least 16 times C_s to limit V_{Cb} to 100 V when the output voltage is 400 V. Practically, C_b should be about 30 times C_s, considering reverse-recovery energy.
4) Snubber inductor L_s should be selected as large as possible to decrease reverse-recovery loss. However, according to the following equation in [14], larger L_s results in lower I_{rr}:

$$I_{rr} \propto \sqrt{I_F \frac{dI_F}{dt}} \propto \sqrt{\frac{I_F}{L_S}}. \tag{23}$$

5) Resonant frequency in (15) should be much greater than switching frequency to ensure correct operation of the snubber cell.

Tradeoffs have to be made when designing L_s, C_s, and C_b. Voltage and current stresses of diodes D_2, D_3, and D_4 are determined by the output voltage and the input current. However, a lower rating is also acceptable due to short snubber operating time. Current stress of the MOSFET is increased by $I_{Ls,p}$; it is much lower than in the hard-switching conditions. Voltage stress of D_1 is increased by $V_{Cb,p}$; since $V_{Cb,p}$ is designed to be lower than 100 V, the increased stress has little effect on cost. Voltage stress of MOSFET and current stress of D_1 are the same as without the snubber cell embedded.

III. The General Snubber Cell for DC/DC Converters

The proposed snubber cell can be seen as the combination of a turn-on snubber cell and a turnoff snubber cell.

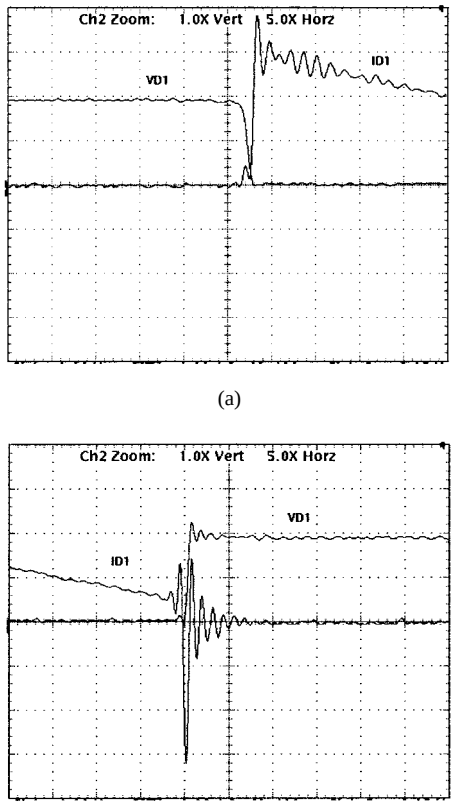

Fig. 11. Commutation waveforms of freewheeling diode without snubber. V_{D1}: 200 V/div; I_{D1}: 2 A/div; Time 1 μs/div. (a) Turn-on transients. (b) Turnoff transients.

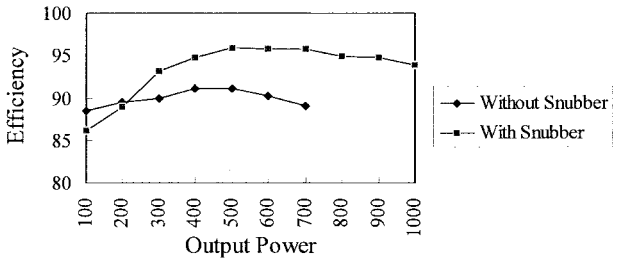

Fig. 12. Efficiency of boost converters with and without snubber.

The turn-on snubber, shown in Fig. 4(a), limits di/dt of the reverse-recovery current by a snubber inductor in series with the freewheeling diode. Two diodes and one capacitor are added to recover the absorbed energy to the output. Most of the turnoff snubbers proposed in the literature use a snubber capacitor parallel to the switch to limit dv/dt of the drain–source voltage. However, in a switching circuit, the voltage across the freewheeling diode always varies with the drain–source voltage of the switch. In other words, dv/dt of the drain–source voltage can also be limited in the turnoff snubber, shown in Fig. 4(b), by paralleling a snubber capacitor to the freewheeling diode. An additional diode is added to isolate the switch from the snubber capacitor. The isolation can prevent the snubber capacitor from being charged through the switch at low load and at no load. It also prevents turn-on switching loss resulting from charge of the snubber capacitor.

The proposed general snubber cell consists of one inductor L_s, two capacitors C_s and C_b, and three diodes D_2, D_3, and D_4. The snubber inductor L_s is placed in series with the freewheeling diode D_1. It is designed to restrict di/dt of the reverse-recovery current to achieve ZCS turn-on. The snubber capacitor C_s is placed in parallel with D_3 and D_4 and isolated by diode D_2. It is designed to restrict dv/dt of the drain–source voltage to achieve ZVS turnoff. ZVS turn-on and turnoff of the freewheeling diode are also obtained. Switching losses and EMI noise during turn-on and turnoff are eliminated by the snubber cell. All energy absorbed in the snubber inductor and snubber capacitor are transferred to the buffer capacitor C_b. Energy recovery is achieved by discharging C_b to the output. Since the snubber cell deals with only small switching transient energy instead of the main power stage energy, the resulting circulating energy is insignificant compared with resonant converters. Snubber operation principles discussed for a boost converter can be extended to other topologies. Six basic nonisolated PWM dc/dc converters: buck, boost, buck-boost, Cúk, Sepic, and Zeta with the proposed snubber cells embedded are shown in Fig. 6. Although circuit size and cost are increased by adding these additional components, it is still tolerable, considering the numerous advantages provided by the snubber cell.

IV. Experimental Results

A prototype of a 1-kW 100-kHz boost converter with the passive lossless snubber has been built to verify the principle of operation and the theoretical analysis. Output voltage is regulated at 380 V dc with the control circuit implemented by an L4981A. The components specifications are listed in Table I. A hard-switching boost converter with same specifications is also built for comparison.

The snubber inductor current, snubber capacitor voltage, and buffer capacitor voltage waveforms are shown in Fig. 7. The commutation waveforms of the MOSFET and the freewheeling diode with the proposed snubber cell embedded are shown in Figs. 8 and 9, respectively. Waveforms of the MOSFET and the freewheeling diode without snubber are shown in Figs. 10 and 11, respectively. The efficiencies of these two circuits are shown in Fig. 12 under different loadings. The maximum efficiency has been measured to be 96% at 700 W.

Waveforms in Fig. 7(a) and (b) are exactly the same as predicted in Fig. 3. Snubber operation analysis is proved to be valid. Comparing Figs. 8(a) and 10(a), it can be seen that di/dt of the drain current is restricted and commutation of the MOSFET is close to ZCS turn-on. The reason for no ZCS is the discharge of the parasitic drain–source capacitance of the MOSFET during the turn-on process. This switching loss mechanism can only be removed by resonant converter techniques or active snubbers. Comparing Figs. 8(b) and 10(b), it can also be seen that dv/dt of the drain–source voltage is restricted and the MOSFET commutates at ZVS turnoff. Fig. 9(a) and (b) shows that the freewheeling diode is also commutated at ZVS turn-on and turnoff. Switching transients of the freewheeling diode are significantly improved compared with the hard-switching counterpart shown in Fig. 11(a) and (b).

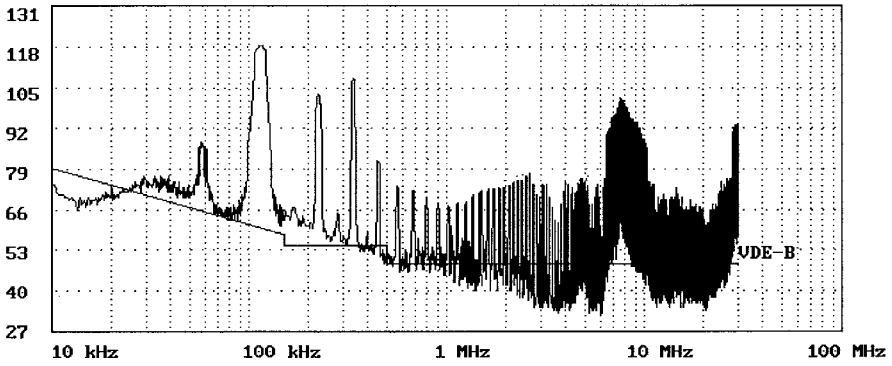

Fig. 13. Total EMI noise of the boost converter with snubber (10 KHz–30 MHz).

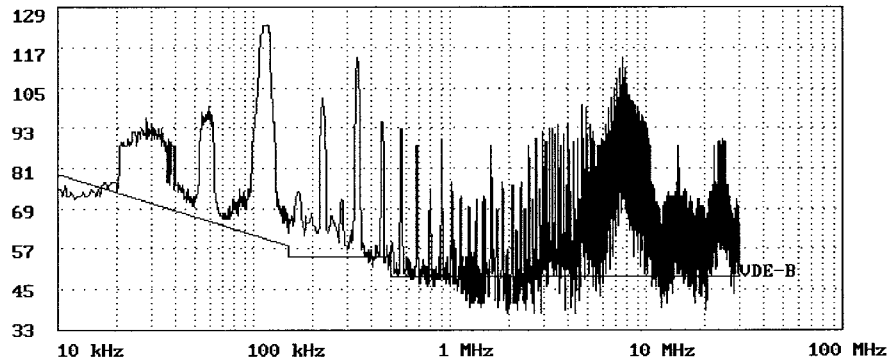

Fig. 14. Total EMI noise of the hard-switching boost converter (10 KHz–30 MHz).

Shown in Figs. 13 and 14 are the total EMI noise measured from 10 KHz to 30 MHz of boost converters with and without the snubber cell, respectively. Limitations of the noise standard, VDE-0871/B, are also shown in both figures. At 100 KHz, the adopted switching frequency, EMI noise of both circuits reaches maximum. It can be seen that the noise at the switching frequency of the boost converter with snubber is approximately 6 dB lower than that of the hard-switching one. Noise at multiples and divisors of the switching frequency are also visibly eliminated. The reduction of the EMI noise should be owed to slower di/dt of the drain current and slower dv/dt of the drain–source voltage.

V. Conclusion

A general passive lossless snubber cell for nonisolated PWM dc/dc converters has been proposed in this paper. The general snubber cell is the combination of a turn-on snubber and a turnoff snubber. Energy recovery is achieved by passive components only. Component values of the snubber inductor, snubber capacitor, and buffer capacitor can be determined by the design rules presented in this paper. Current stress of the MOSFET and voltage stress of the freewheeling diode are also presented clearly. A 1-kW 100-kHz prototype of a boost converter equipped with the snubber has been implemented in the laboratory to verify the analyses above. Experimental waveforms show that the increasing rates of the reverse-recovery current and the drain–source voltage are successfully restricted by the snubber. The MOSFET operates at ZVS turnoff and close to ZCS turn-on; the freewheeling diode operates at ZVS turn-on and turnoff.

References

[1] A. Pietkiewicz and D. Tollik, "Snubber circuit and mosfet paralleling considerations for high power boost-based power-factor correctors," in *Proc. INTELEC'95*, 1995, pp. 41–45.
[2] A. Elasser and D. A. Torry, "Soft switching active snubbers for dc/dc converters," *IEEE Trans. Power Electron.*, vol. 11, pp. 710–722, Sept. 1996.
[3] G. Hua and F. C. Lee, "Soft-switching techniques in PWM converters," *IEEE Trans. Ind. Electron.*, vol. 42, pp. 595–603, Dec. 1995.
[4] R. L. Lin and F. C. Lee, "Novel zero-current-switching-zero-voltage-switching converters," in *Proc. PESC'96*, 1996, pp. 438–442.
[5] R. Streit and D. Tollik, "High efficiency telecom rectifier using a novel soft-switched boost-based input current shaper," in *Proc. INTELEC'91*, 1991, pp. 720–726.
[6] S. J. Finney, B. W. Williams, and T. C. Green, "The RCD snubber revisited," in *Conf. Rec. IEEE-IAS Annu. Meeting*, 1993, pp. 1267–1273.
[7] G. A. Karvelis and S. N. Manias, "Fixed-frequency buck-boost zero-voltage-switched quasiresonant converter," *Proc. IEE—Elect. Power Applicat.*, vol. 142, no. 5, pp. 289–296, Sept. 1995.
[8] W. Gu and K. Harada, "A novel self-excited forward dc-dc converter with zero-voltage-switched resonant transitions using saturable core," *IEEE Trans. Power Electron.*, vol. 10, pp. 131–141, Mar. 1995.
[9] M. Ferranti, P. Ferraris, A. Fratta, and F. Profumo, "Solar energy supply system for induction motors and various loads," presented at INTELEC'89, 1989, Paper 15.7.
[10] N. Machin and T. Vescovi, "Very high efficiency techniques and their selective application to the design of a 70 A rectifier," in *Proc. INTELEC'93*, 1993, pp. 126–133.
[11] J. Lambert, J. Vieira, L. C. Freitas M. Vilela, and V. Farias, "A boost PWM soft-single-switched converter without stresses of voltage and current," in *Proc. APEC'96*, 1996, pp. 469–474.

[12] X. He, B. W. Williams, S. J. Finney, Z. Qian, and T. C. Green, "New snubber circuit with passive energy recovery for power inverters," *Proc. IEE—Elect. Power Applicat.*, vol. 143, no. 5, pp. 403–408, Sept. 1996.
[13] G. Carli, "Harmonic distortion reduction schemes for a new 100 A–48 V power supply," in *Proc. INTELEC'92*, 1992, pp. 524–531.
[14] N. Mohan, T. Undeland, and W. Robbins, *Power Electronics: Converters, Applications and Design*. New York: Wiley, 1989, pp. 462–467.

Ching-Jung Tseng was born in Taipei, Taiwan, R.O.C., in 1972. He received the B.S. and Ph.D. degrees in electrical engineering from National Taiwan University, Taipei, Taiwan, R.O.C., in 1994 and 1998, respectively.

His current research is focused on the design of soft-switching topologies and power factor correction.

Chern-Lin Chen (S'86–M'90) was born in Taipei, Taiwan, R.O.C., in 1962. He received the B.S. and Ph.D. degrees in electrical engineering from National Taiwan University, Taipei, Taiwan, R.O.C., in 1984 and 1987, respectively.

Following receipt of the Ph.D. degree, he joined the Department of Electrical Engineering, National Taiwan University, where he is currently a Professor. His current research interests lie in the areas of analysis, design, and application of power electronics converters and motor drives.